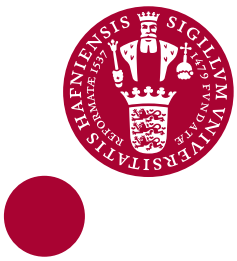

Cortex-wide Changes in Extracellular Potassium Ions Parallel Brain State Transitions in Awake Behaving Mice

Rasmussen, Rune; Nicholas, Eric; Petersen, Nicolas Caesar; Dietz, Andrea Grostol; Xu, Qiwu; Sun, Qian; Nedergaard, Maiken

Published in:
Cell Reports

DOI:
10.1016/j.celrep.2019.06.082

Publication date:
2019

Document version
Publisher's PDF, also known as Version of record

Article

Cell Reports

Cortex-wide Changes in Extracellular Potassium Ions Parallel Brain State Transitions in Awake Behaving Mice

Graphical Abstract

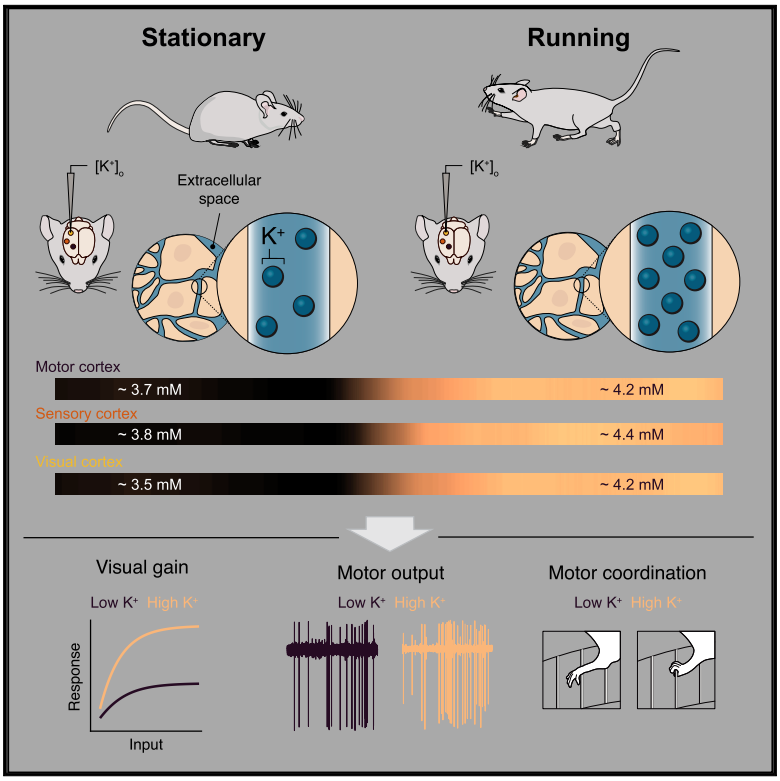

Highlights

- Behavioral state transitions is paralleled by a cortex-wide increase in $[K^+]_o$
- Increased $[K^+]_o$ depolarizes cortical neurons and amplifies their excitability *in vitro*
- State-dependent visual gain modulation is recreated by local changes in $[K^+]_o$
- Increasing motor cortical $[K^+]_o$ enhances L5 spiking and improves motor performance

Authors

Rune Rasmussen, Eric Nicholas, Nicolas Caesar Petersen, Andrea Grostøl Dietz, Qiwu Xu, Qian Sun, Maiken Nedergaard

Correspondence

runerasmussen@dandrite.au.dk (R.R.), maiken_nedergaard@urmc.rochester.edu (M.N.)

In Brief

The brain's response to sensory input is strikingly modulated by behavioral state, but the mechanisms governing this effect remain unclear. Rasmussen et al. show that behavioral transitions are accompanied by stereotypical cortex-wide changes in extracellular K^+, capable of regulating sensory and motor processing through the modulation of neural activity.

Rasmussen et al., 2019, Cell Reports *28*, 1182–1194
July 30, 2019
https://doi.org/10.1016/j.celrep.2019.06.082

CellPress

OPEN ACCESS
CellPress

Cell Reports
Article

Cortex-wide Changes in Extracellular Potassium Ions Parallel Brain State Transitions in Awake Behaving Mice

Rune Rasmussen,[2,3,*] Eric Nicholas,[1,4] Nicolas Caesar Petersen,[2] Andrea Grostøl Dietz,[2] Qiwu Xu,[1] Qian Sun,[1] and Maiken Nedergaard[1,2,5,*]

[1]Center for Translational Neuromedicine, University of Rochester Medical Center, Rochester, NY 14642, USA
[2]Center for Translational Neuromedicine, Faculty of Health and Medical Sciences, University of Copenhagen, 2200 Copenhagen N, Denmark
[3]Present address: The Danish Research Institute of Translational Neuroscience – DANDRITE, Nordic EMBL Partnership for Molecular Medicine, Department of Biomedicine, Aarhus University, 8000 Aarhus C, Denmark
[4]Present address: Cognitive Neurophysiology Lab, University of Rochester Medical Center, Rochester, NY 14642, USA
[5]Lead Contact
*Correspondence: runerasmussen@dandrite.au.dk (R.R.), maiken_nedergaard@urmc.rochester.edu (M.N.)
https://doi.org/10.1016/j.celrep.2019.06.082

SUMMARY

Brain state fluctuations modulate sensory processing, but the factors governing state-dependent neural activity remain unclear. Here, we tracked the dynamics of cortical extracellular K^+ concentrations ($[K^+]_o$) during awake state transitions and manipulated $[K^+]_o$ in slices, during visual processing, and during skilled motor execution. When mice transitioned from quiescence to locomotion, $[K^+]_o$ increased by 0.6–1.0 mM in all cortical areas analyzed, and this preceded locomotion by 1 s. Emulating the state-dependent $[K^+]_o$ increase in cortical slices caused neuronal depolarization and enhanced input-output transformation. *In vivo*, locomotion increased the gain of visually evoked responses in layer 2/3 of visual cortex; this effect was recreated by imposing a $[K^+]_o$ increase. Elevating $[K^+]_o$ in the motor cortex increased movement-induced neuronal spiking in layer 5 and improved motor performance. Thus, $[K^+]_o$ increases in a cortex-wide state-dependent manner, and this $[K^+]_o$ increase affects both sensory and motor processing through the dynamic modulation of neural activity.

INTRODUCTION

Behavioral responses to sensory inputs are powerfully influenced by the ongoing and constantly fluctuating internal brain state (Harris and Thiele, 2011; Lee and Dan, 2012; Poulet and Crochet, 2019). Yet, it is unclear how the brain can effectively switch between and maintain different brain states. During movement and periods of increased arousal, the cerebral cortex transitions into an active, desynchronized state compared to the slow, synchronized state during quiescence (Bennett et al., 2013; Crochet and Petersen, 2006; Polack et al., 2013; Poulet and Petersen, 2008). The active cortical state has a substantial functional impact, as it is accompanied by marked changes in sensory processing (Castro-Alamancos, 2004; Crochet and Petersen, 2006; Otazu et al., 2009). For example, visually evoked responses in the visual cortex are amplified when mice are locomoting and neurons are in a depolarized and desynchronized state (Bennett et al., 2013; Dadarlat and Stryker, 2017; Neske and McCormick, 2018; Niell and Stryker, 2010; Polack et al., 2013), and this is linked to enhanced visual detection performance (Bennett et al., 2013).

Despite substantial progress, our knowledge about the mechanisms mediating state-dependent modulation of sensory processing remains incomplete. A variety of factors could be orchestrating the neural activity changes reported in the cortex of awake behaving mice: thalamic excitatory inputs (Poulet et al., 2012), disinhibition (Fu et al., 2014), or neuromodulator signaling (Eggermann et al., 2014; Polack et al., 2013; Schiemann et al., 2015). However, given the cortex-wide nature of awake brain states, alternative non-synaptic mechanisms could be acting over a slower timescale to support the stability of distinct states. The extracellular ionic environment, which surrounds all neurons, is a possible candidate mechanism for this. A number of recent studies have begun to challenge the notion that ion changes are merely epiphenomenal; extracellular ion concentration changes have been causally implicated in the generation of rhythmic locomotor activity in the spinal cord (Brocard et al., 2013), the sleep-wake cycle (Ding et al., 2016; Rasmussen et al., 2017), the emergence of neuronal oscillations (Bazhenov et al., 2004; Krishnan et al., 2018), and sleep duration, and architecture is critically influenced by K^+ channels (Cirelli, 2009; Cirelli et al., 2005; Tatsuki et al., 2016; Yoshida et al., 2018). Because the concentration of extracellular K^+ ions strongly modulates the membrane potential (V_m), excitability and spiking of neurons (Balestrino et al., 1986; Brocard et al., 2013; Fröhlich et al., 2008; Octeau et al., 2019; Poolos et al., 1987; Shih et al., 2013; Tong et al., 2014; Wang et al., 2012), $[K^+]_o$ changes could theoretically be involved in driving the neural activity transition from quiet to active wakefulness (Rasmussen et al., 2017). However, the dynamics of cortical $[K^+]_o$ during awake brain states and their influence on neuronal processing remain to be established.

Here, we used K^+-sensitive microelectrodes to characterize the dynamics of $[K^+]_o$ in multiple cortical areas and layers during awake brain state transitions and manipulated $[K^+]_o$ in slices, during visual processing, and during skilled motor behavior. Our results show that $[K^+]_o$ increases globally by ~0.7 mM across the cortex when mice transition from quiescence to locomoting; this $[K^+]_o$ rise precedes locomotor onset by ~1 s, remains elevated until the offset of locomotion, and is sensitive to suppression of local excitatory transmission. The state-dependent $[K^+]_o$ shift is sufficient to tonically depolarize cortical neurons and enhance their input-output transformation in slices. In layer (L) 2/3 of the visual cortex, locomotion multiplicatively increases the gain of visually evoked neuronal responses, and this effect is fully recreated by increasing $[K^+]_o$ locally, while raising $[K^+]_o$ in the motor cortex increases motor-related L5 spiking and improves precise motor behavior. Together, these data suggest that state-dependent cortex-wide changes in $[K^+]_o$ are capable of regulating sensory and motor processing in behaving animals through the modulation of neural activity.

RESULTS

Motor Cortical $[K^+]_o$ Consistently Increases Prior to Behavioral State Change

A well-characterized state change occurs across widespread cortical areas when mice transition from being stationary to running (Bennett et al., 2013; McGinley et al., 2015; Polack et al., 2013; Reimer et al., 2014; Schiemann et al., 2015). Does $[K^+]_o$ exhibit systematic changes during this transition? Mice were accustomed to spontaneously running on a cylindrical treadmill, while $[K^+]_o$ and the local field potential (LFP) were recorded in L2/3 of the motor cortex (Figure 1A). Mice freely alternated between running and being stationary, with the latter defined as periods when the mouse did not rotate the treadmill (running velocity < 1 cm/s). During recording sessions from six animals, $[K^+]_o$ spanned a range of 2.7 to 5.4 mM (median = 3.5 mM) and was on average 3.7 ± 0.17 mM (mean ± SEM); notably, $[K^+]_o$ was non-normally distributed and skewed to the right (Figure 1B; $p < 0.001$, one-sample Kolmogorov-Smirnov test; skewness = 1.31, kurtosis = 8.35). We investigated if this skewness was related to the behavioral state of the animal. Strikingly, running periods tightly correlated with increased $[K^+]_o$ in all animals (Figures 1C–1E; $r = 0.74$, $p < 0.001$, Pearson's correlation coefficient), although the absolute $[K^+]_o$ range varied slightly between animals (Figure 1C). $[K^+]_o$ remained elevated at a plateau throughout running, before reverting to baseline levels when running ceased, and $[K^+]_o$ changes were highly reliable across running periods (Figures 1D and 1E). As expected, transitions from being stationary to running were associated with a clear neuronal state change: 1−4 Hz LFP components greatly reduced during running (Figure 1D) (Bennett et al., 2013; Polack et al., 2013; Reimer et al., 2014). Next, we systematically determined $[K^+]_o$ before and during running. This revealed a notable trend for higher $[K^+]_o$ during running (Figure 1F); on average, $[K^+]_o$ increased 0.77 ± 0.09 mM when mice were running (Figure 1G; $p < 0.001$, Wilcoxon signed-rank test). We found no correlation between running speed and $[K^+]_o$ ($r = 0.07$, $p \geq 0.05$, Pearson's correlation coefficient). From Figures 1D and 1C, the rise in $[K^+]_o$ appears to precede the onset of running. We investigated the temporal relationship between $[K^+]_o$ and running onset, determining when $[K^+]_o$ increased above baseline ($[K^+]_o$ threshold = stationary mean + 1 × SD) relative to running onset. $[K^+]_o$ began increasing 1.15 ± 0.1 s prior to the onset of running (Figures 1H and 1I; $p < 0.001$, one-sample signed-rank test). These data suggest that, in L2/3 of the motor cortex, running periods are reliably associated with a ~0.7 mM $[K^+]_o$ increase that precedes running onset, which is maintained throughout running (Table S1). Hence, changes in $[K^+]_o$ accompany motor cortical state transitions and exhibit distinct plateaus that last for the duration of each period of locomotor activity.

Cortical $[K^+]_o$ Increases Globally during Behavioral State Change

The motor cortex plays a central role in voluntary movements, and motor cortical neurons change their spike rate during movement (Armstrong and Drew, 1984; Dombeck et al., 2009; Schiemann et al., 2015). Increased spiking can elevate $[K^+]_o$ (Hounsgaard and Nicholson, 1983), implying that our findings may be exclusive to motor areas. We therefore investigated if state-dependent $[K^+]_o$ increases are indeed confined to the motor cortex or whether they are a global cortical phenomenon. To address this, we repeated the previous experiment in the visual cortex, an area not involved in movement execution. Recordings in visual cortex L2/3 revealed that running periods here are also associated with increased $[K^+]_o$ (Figure 2A). As observed in the motor cortex, we found a strong trend for elevated $[K^+]_o$ during running (Figure 2B). $[K^+]_o$ increased on average 0.62 ± 0.05 mM when mice went from being stationary to running (Figure 2C; $p < 0.001$, Wilcoxon signed-rank test), and $[K^+]_o$ started to increase 0.9 ± 0.12 s prior to running onset (Figures 2D and 2E; $p < 0.001$, one-sample signed-rank test). Another set of recordings performed in L2/3 of the sensory cortex revealed very similar patterns (Figure S1). $[K^+]_o$ dynamics in L2/3 of the visual, sensory, and motor cortex were thus strikingly similar (Table S1). We also measured $[K^+]_o$ while changing the K^+ content of the artificial cerebrospinal fluid (ACSF) bathing the visual cortex, from the standard 3.5 mM K^+ to either 5 or 0 mM K^+, in order to manipulate baseline $[K^+]_o$ (Figure S2). We found that $[K^+]_o$ increased 0.75 ± 0.05 mM and 0.53 ± 0.03 mM with 5 and 0 mM K^+ ACSF, respectively, when mice transitioned from being stationary to running (Figure S2; $p < 0.001$ for both comparisons, Wilcoxon signed-rank test). Thus, state-dependent $[K^+]_o$ increases persisted across a wide range of baseline $[K^+]_o$ levels. Here, it is important to note that $[K^+]_o$ increased more with 5 compared to 3.5 mM K^+ ACSF ($p < 0.05$, Wilcoxon rank-sum test), and increased less with 0 compared to 3.5 mM K^+ ACSF ($p < 0.01$, Wilcoxon rank-sum test), suggesting that baseline $[K^+]_o$ plays a role in the magnitude of state-dependent $[K^+]_o$ rises.

State transitions are not exclusive to superficial cortical layers; in L4 and L5, neurons also transition into a desynchronized state during movement (McGinley et al., 2015; Schiemann et al., 2015; Zhao et al., 2016). Therefore, to further elucidate the link between brain state and $[K^+]_o$ dynamics, we recorded $[K^+]_o$ in L5 of the visual cortex. Again, $[K^+]_o$ reliably increased prior to running onset, with a concomitant decrease of 1−4 Hz LFP fluctuations (Figure 2F). L5 $[K^+]_o$ increased on average 1.05 ± 0.09 mM when

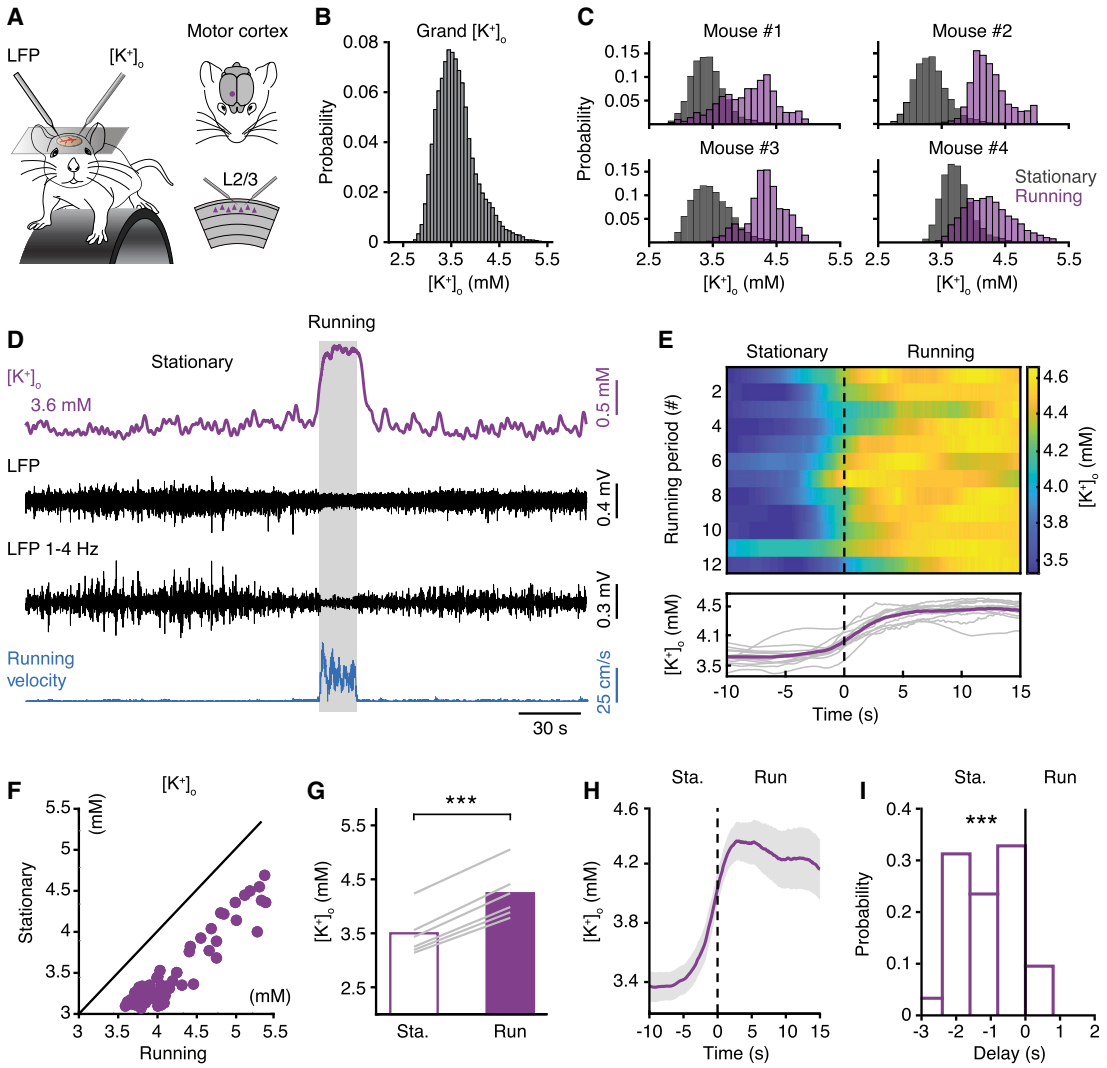

Figure 1. Motor Cortex $[K^+]_o$ Consistently Increases Prior to and during Behavioral State Change

(A) Awake head-fixed mice spontaneously stood or ran on a cylindrical treadmill while $[K^+]_o$ and LFP recordings were made from motor cortex L2/3.

(B) Grand distribution of $[K^+]_o$ recorded from 6 awake intermittently running mice ($p < 0.001$, one-sample Kolmogorov-Smirnov test; skewness = 1.31, kurtosis = 8.35).

(C) Comparison of $[K^+]_o$ distribution during stationary (gray) and running (purple) periods from 4 example mice ($p < 0.001$ for all mice, two-sample Kolmogorov-Smirnov test).

(D) Example traces of $[K^+]_o$, broadband LFP, 1–4 Hz LFP, and running velocity; gray shading highlights running period.

(E) Top: color map depicting $[K^+]_o$ dynamics from being stationary to running during multiple running periods for a single mouse. Bottom: corresponding $[K^+]_o$ traces; individual periods are in gray and average is in purple.

(F) Pairs of $[K^+]_o$ during stationary and running periods.

(G) Comparison of $[K^+]_o$ during stationary and running periods. ***$p < 0.001$, n = 69 periods, N = 6 mice, Wilcoxon signed-rank test; lines represent average $[K^+]_o$ shift for each mouse.

(H) Average $[K^+]_o$ trace during transition from being stationary to running; shading indicates SEM.

(I) Histogram depicting distribution of onset of $[K^+]_o$ increase relative to running onset. ***$p < 0.001$, n = 69 periods, N = 6 mice, one-sample signed-rank test. See also Table S1.

mice went from being stationary to running (Figures 2G and 2H; $p < 0.001$, Wilcoxon signed-rank test) and rose 0.92 ± 0.1 s before running onset (Figures 2I and 2J; $p < 0.001$, one-sample signed-rank test). Thus, the state-dependent $[K^+]_o$ changes in the visual, sensory, and motor cortex were identical in L2/3 ($p \geq 0.05$, Kruskal-Wallis test), but $[K^+]_o$ increases were higher in L5 of the visual cortex ($p < 0.01$, Kruskal-Wallis test). These experiments suggest that a 0.5–1 mM increase in $[K^+]_o$ parallels the transition from quiescence to locomotion (Table S1). The rise in $[K^+]_o$ is maintained across a range of baseline $[K^+]_o$ levels, is shared across cortical areas, and thus appears to be a robust global cortical phenomenon.

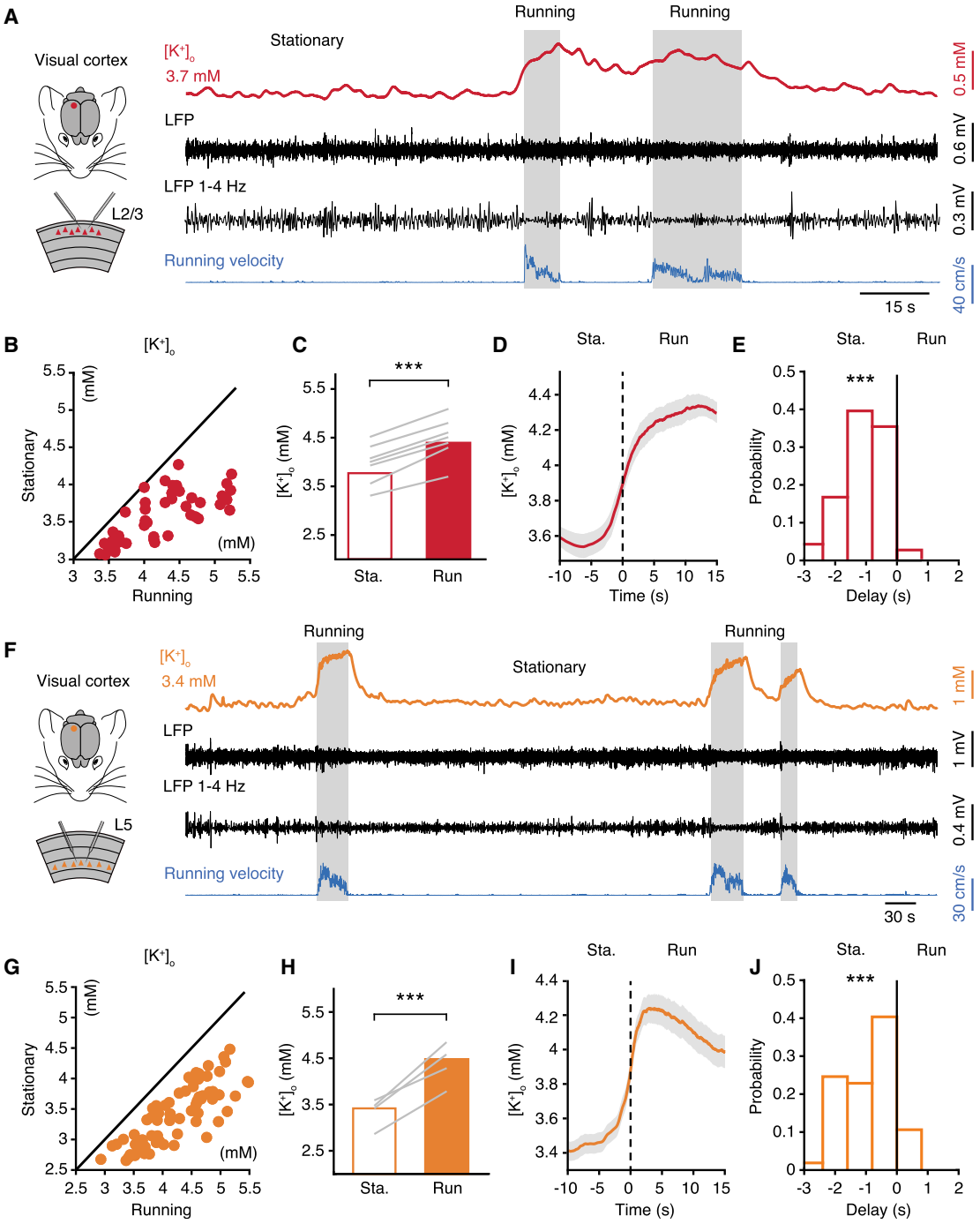

Figure 2. Cortical $[K^+]_o$ Increases Globally during Behavioral State Change

(A) Example traces of visual cortex L2/3 $[K^+]_o$, broadband LFP, 1–4 Hz LFP, and running velocity; gray shading highlights running periods.

(B) Pairs of $[K^+]_o$ during stationary and running periods.

(C) Comparison of $[K^+]_o$ during stationary and running periods. ***$p < 0.001$, n = 48 periods, N = 6 mice, Wilcoxon signed-rank test; lines represent average $[K^+]_o$ shift for each mouse.

(D) Average $[K^+]_o$ trace during transition from stationary to running; shading indicates SEM.

(E) Histogram depicting distribution of onset of $[K^+]_o$ increase relative to running onset. ***$p < 0.001$, n = 48 periods, N = 6 mice, one-sample signed-rank test.

(F) Same as in (A), but for L5.

(G) Same as in (B), but for L5.

(legend continued on next page)

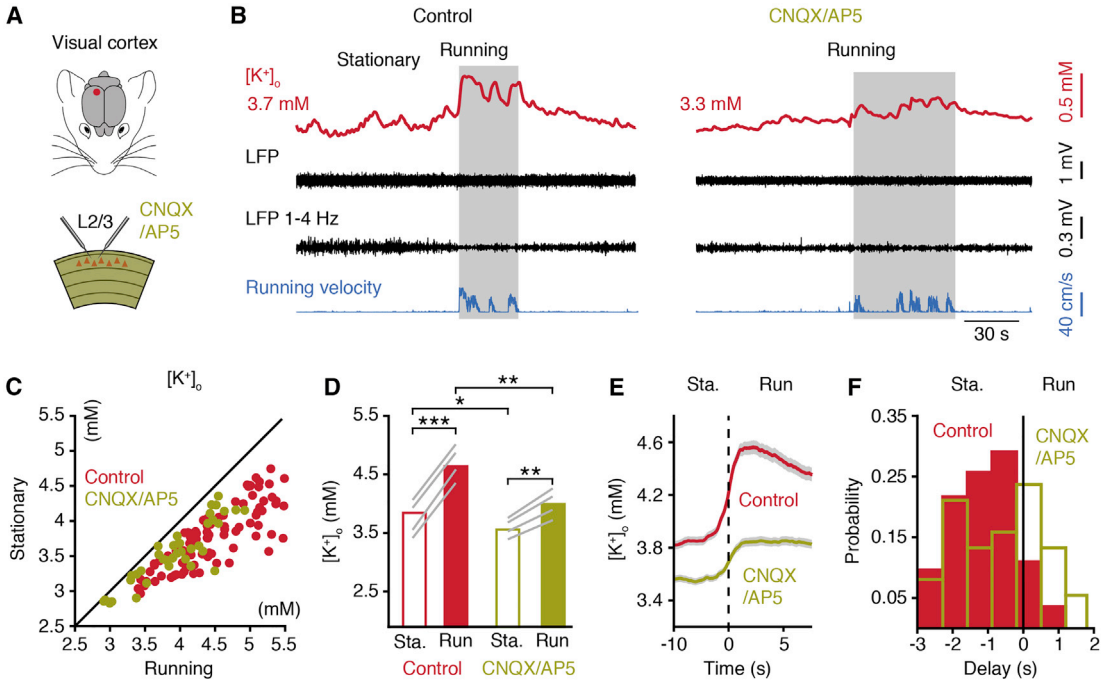

Figure 3. Local Excitatory Transmission Contributes to State-Dependent $[K^+]_o$ Changes

(A) $[K^+]_o$ and LFP recordings were made from L2/3 of the visual cortex before and after application of glutamatergic receptor antagonists CNQX and AP5.

(B) Example traces of visual cortex L2/3 $[K^+]_o$, broadband LFP, 1–4 Hz LFP, and running velocity before and after application of CNQX and AP5; gray shading highlights running periods.

(C) Pairs of $[K^+]_o$ during stationary and running periods.

(D) Comparison of $[K^+]_o$ during stationary and running periods before and after CNQX and AP5 application. *$p < 0.05$, **$p < 0.01$, ***$p < 0.001$, n = 31 and 32 periods for control and CNQX and AP5, respectively; N = 4 mice; Wilcoxon signed-rank test; lines represent average $[K^+]_o$ shift for each mouse.

(E) Average $[K^+]_o$ trace during transition from being stationary to running before and after CNQX and AP5; shading indicates SEM.

(F) Histogram depicting distribution of onset of $[K^+]_o$ increase relative to running onset before ($p < 0.001$, n = 31 periods, N = 4 mice, one-sample signed-rank test) and after ($p \geq 0.05$, n = 32 periods, N = 4 mice, one-sample signed-rank test) CNQX and AP5.

See also Figures S3 and S4.

Local Excitatory Transmission Contributes to State-Dependent Changes in $[K^+]_o$

To explore what mechanisms govern the state-dependent increase in $[K^+]_o$, we suppressed local excitatory activity. We recorded $[K^+]_o$ and the LFP in L2/3 of the visual cortex in spontaneously running mice before (control) and after topical application of 6-cyano-7-nitroquinoxaline-2,3-dione (CNQX) and (2R)-amino-5-phosphonovaleric acid (AP5), blocking α-amino-3-hydroxy-5-methyl-4-isoxazolepropionic acid (AMPA) and N-Methyl-D-aspartate (NMDA) receptors, respectively (Figure 3A). CNQX and AP5 potently reduced broadband LFP power by more than 60% (Figure S3). Following CNQX and AP5 addition, baseline $[K^+]_o$ decreased 0.27 ± 0.18 mM compared to control conditions ($p < 0.05$, Wilcoxon signed-rank test), and running-associated $[K^+]_o$ increases were diminished (Figures 3B–3D). After application of CNQX and AP5, the $[K^+]_o$ increase was reduced by ~42% (to 0.4 ± 0.15 mM) compared to control conditions (Figure 3D; $p < 0.01$, Wilcoxon signed-rank test), and the $[K^+]_o$ onset occurred 0.17 ± 0.4 s before running onset (Figures 3E and 3F; $p \geq 0.05$, one-sample signed-rank test). To further explore the relationship between local neuronal activity and $[K^+]_o$ dynamics, we related multi-unit activity (MUA) spiking to $[K^+]_o$ during behavioral state changes. MUA spiking and $[K^+]_o$ was well correlated (Figure S4; $r = 0.63$, $p < 0.001$, Pearson's correlation coefficient), and cross-correlation analysis showed that $[K^+]_o$ was delayed by ~1.1 s relative to MUA spiking (Figure S4). These results suggest that behavioral state-dependent $[K^+]_o$ changes in the cortex are sensitive to the suppression of local neuronal activity and correlated with periods of increased neural spiking.

Running-Associated $[K^+]_o$ Increase Causes Tonic Depolarization of Cortical Neurons

Next we asked what electrophysiological consequences might occur if we raised $[K^+]_o$ to a similar magnitude as that observed when mice transition from being stationary to running (Figures 1, 2, and 3). To explore this, we used whole-cell patch-clamp

(H) Same as in (C), but for L5. ***$p < 0.001$, n = 76 periods, N = 4 mice, Wilcoxon signed-rank test.

(I) Same as in (D), but for L5.

(J) Same as in (E), but for L5. ***$p < 0.001$, n = 76 periods, N = 4 mice, one-sample signed-rank test.

See also Figures S1 and S2 and Table S1.

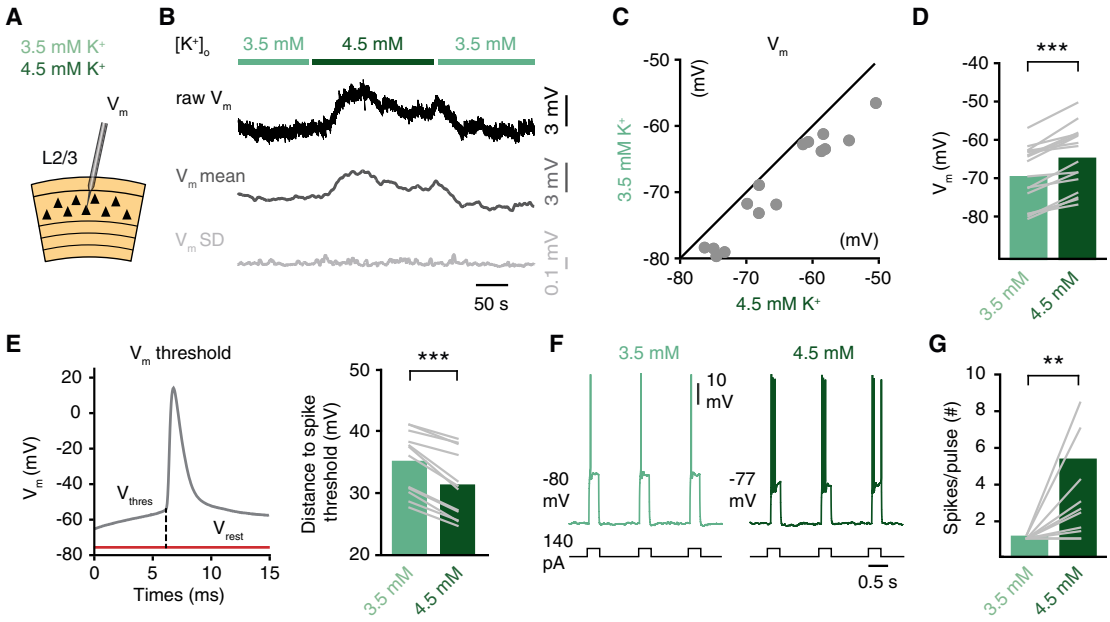

Figure 4. A Running-Associated $[K^+]_o$ Increase Causes Tonic Depolarization of Cortical Neurons

(A) Whole-cell patch-clamp recordings were obtained from cortical L2/3 pyramidal neurons in slices. The slices were superfused with 3.5 or 4.5 mM K^+ ACSF.

(B) Example traces of raw V_m, mean V_m, and V_m SD when shifting between 3.5 and 4.5 mM K^+.

(C) Pairs of V_m in 3.5 and 4.5 mM K^+.

(D) Comparison of V_m in 3.5 and 4.5 mM K^+. ***$p < 0.001$, n = 16 cells, N = 5 mice, Wilcoxon signed-rank test; lines represent V_m shift for each cell.

(E) Left: distance to spike threshold was measured as distance from resting V_m to the kink in the spike waveform. Right: comparison of distance to spike threshold in 3.5 and 4.5 mM K^+. ***$p < 0.001$, n = 12 cells, N = 5 mice, Wilcoxon signed-rank test; lines represent distance to threshold shift for each cell.

(F) Example V_m recordings during current injections in 3.5 or 4.5 mM K^+ for the same cell.

(G) Comparison of excitability in 3.5 and 4.5 mM K^+. **$p < 0.01$, n = 10 cells, N = 4 mice, Wilcoxon signed-rank test; lines represent excitability shift for each cell.

See also Figure S5.

recordings in cortical slices (Figure 4A). We obtained current-clamp recordings from L2/3 pyramidal neurons and measured resting V_m: first in 3.5 mM K^+ ACSF and then switching to 4.5 mM K^+, causing a 0.7 mM $[K^+]_o$ increase (Figure S5). Importantly, we are aware that the magnitude of state-dependent cortical $[K^+]_o$ increases varies between 0.5–1 mM, depending on the baseline $[K^+]_o$ level (Figures 1, 2, S1, and S2). For this experiment we chose to recapitulate the $[K^+]_o$ change observed when baseline $[K^+]_o$ is ~3.5 mM (Figures 1 and 2), a $[K^+]_o$ within normal physiological range (Somjen, 2004). Experiments were performed in the presence of fast glutamatergic and GABAergic transmission antagonists (Cotel et al., 2013) to isolate the specific effects of changing $[K^+]_o$. When increasing $[K^+]_o$, we measured a V_m depolarization of 4.2 ± 2.1 mV (Figures 4B–4D; $p < 0.001$, Wilcoxon signed-rank test). Hence, increasing $[K^+]_o$ decreased the distance to spike threshold (Figure 4E; $p < 0.001$, Wilcoxon signed-rank test) without significantly affecting spike threshold (−46.7 ± 1.7 mV and −47.4 ± 1.8 mV in 3.5 and 4.5 mM K^+, respectively, $p \geq 0.05$, Wilcoxon signed-rank test), input resistance (112 ± 4.8 MΩ and 105 ± 3.87 MΩ in 3.5 and 4.5 mM K^+, respectively, $p \geq 0.05$, Wilcoxon signed-rank test), or V_m variance (28.7 ± 9.2 μV^2 and 22.7 ± 6.9 μV^2 in 3.5 and 4.5 mM K^+, respectively, $p \geq 0.05$, Wilcoxon signed-rank test).

V_m shifts profoundly influence neuronal input-output transformations (Chance et al., 2002; Murphy and Miller, 2003). We asked what effect the V_m depolarization, driven by $[K^+]_o$, has on input-output transformations in cortical neurons. To test this, we performed somatic current injection experiments (Figure 4F), allowing a way of probing the effect of depolarizing currents arriving at the soma on spike output (Cotel et al., 2013; Schiemann et al., 2015). Raising $[K^+]_o$ notably increased excitability, measured by the number of elicited spikes (Figure 4G; $p < 0.01$, Wilcoxon signed-rank test). The average spike rate was on the order of three times higher in 4.5 mM K^+ compared to 3.5 mM K^+ (Figure 4G). These results suggest that $[K^+]_o$ changes of the same magnitude as measured during behavioral state transitions *in vivo* are capable of causing notable changes in the biophysical properties of cortical pyramidal neurons.

Visually Evoked Responses Are Multiplicatively Gained in the Visual Cortex during Running

Previous work demonstrated that visually evoked responses in the visual cortex are gained when mice are aroused (Bennett et al., 2013; Dadarlat and Stryker, 2017; Neske and McCormick, 2018; Niell and Stryker, 2010; Polack et al., 2013). However, the detailed mechanisms producing state-dependent gain modulation in the visual cortex are incompletely understood. To probe this, we first measured visually evoked potentials (VEPs) in L2/3 of the visual cortex in awake, spontaneously running mice. To elicit responses, we delivered a 20 ms flash stimulus

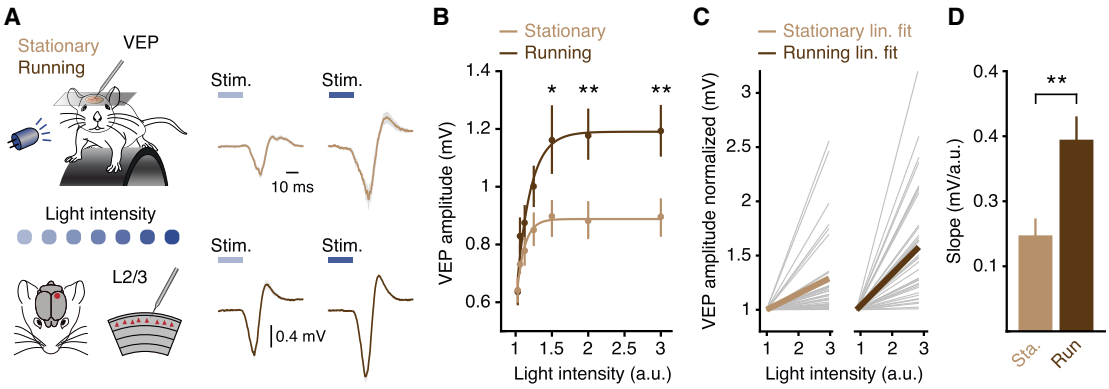

Figure 5. Visually Evoked Responses Are Multiplicatively Gained in the Visual Cortex during Running

(A) Left: VEPs were elicited in visual cortex L2/3 in awake mice exhibiting spontaneous transitions between being stationary and running. Right: example VEP traces elicited by light intensities 1 and 2 while the mouse was stationary (top) or running (bottom); blue bars denote visual stimulation; shading indicates SEM.

(B) VEP amplitude as a function of light intensity for stationary and running. *$p < 0.05$, **$p < 0.01$, $n = 48$ recordings, $N = 8$ mice, Wilcoxon signed-rank test; error bars are mean ± SEM and solid lines are sigmoid fit.

(C) Linear function fits to the normalized VEP amplitude as a function of light intensity for stationary and running; individual fits are in gray and average is colored.

(D) Bar plot comparing slopes of linear function fits. **$p < 0.01$, $n = 48$ recordings, $N = 8$ mice, Wilcoxon signed-rank test; error bars indicate SEM.

at different light intensities (Figure 5A). Trials were post hoc categorized into "stationary" and "running" based on the locomotor activity leading up to the visual stimulus (see STAR Methods). We found marked effects of the behavioral state on the amplitude of VEPs, with larger responses being evoked during running compared to being stationary (Figure 5B; $p < 0.05$, Wilcoxon signed-rank test). The slopes of the input-output curves were steeper in the running state compared to the stationary state (Figure 5C; $p < 0.01$, Wilcoxon signed-rank test). Thus, these data add evidence to the state-dependent multiplicative gain modulation previously reported in the visual cortex (Dadarlat and Stryker, 2017; Neske and McCormick, 2018; Polack et al., 2013).

Increasing Local $[K^+]_o$ Recreates State-Dependent Gain Modulation in the Visual Cortex

Next, we investigated if $[K^+]_o$ might be involved in producing the observed multiplicative gain modulation. *In vivo*, subtle V_m depolarization can cause gain modulation (Murphy and Miller, 2003). Intriguingly, raising $[K^+]_o$ by ~0.7 mM, emulating the $[K^+]_o$ increase from being stationary to running (Figures 1, 2, and 3), depolarized cortical neurons by 4 mV in slices (Figure 4), inviting the hypothesis that $[K^+]_o$ changes contribute to cortical gain modulation. To test this, we recorded VEPs in awake, stationary mice while manipulating $[K^+]_o$ (Figure 6A). The visual cortex was covered with ACSF containing either 3.5 or 5 mM K^+, the latter creating an effective ~0.7 mM $[K^+]_o$ increase in L2/3 (Figure S5). Manipulating $[K^+]_o$ caused notable effects on VEP amplitudes, with larger responses being evoked with 5 mM K^+ compared to 3.5 mM K^+ (Figure 6B; $p < 0.001$, Wilcoxon signed-rank test). Strikingly, the slopes of the input-output curves were steeper when $[K^+]_o$ was increased (Figure 6C; $p < 0.001$, Wilcoxon signed-rank test), thus fully recreating the multiplicative gain modulation observed during running. This result suggests that, in the active state, visual responses are multiplicatively gained in the visual cortex, and this gain modulation could be, at least in part, driven by $[K^+]_o$ increases. Furthermore, locally raising $[K^+]_o$ replicated state-dependent gain modulation, suggesting that sensory gain can be controlled within the cortex independent of extracortical changes.

Increasing $[K^+]_o$ in the Motor Cortex Improves Motor Performance and Amplifies L5 Spiking

Motor cortical output might not be essential for simple locomotion in quadrupeds (Drew et al., 2004; Kiehn, 2016; Miri et al., 2017; Orlovsky et al., 1999), but it may be more pertinent to behaviors requiring skilled motor coordination (Drew and Marigold, 2015; Lemke et al., 2019; Miri et al., 2017; Schiemann et al., 2015). We observed reliable $[K^+]_o$ increases in motor cortex with running (Figure 1). Here, we sought to test if increasing $[K^+]_o$ in the motor cortex might have behavioral consequences. For this, we employed a cylindrical treadmill equipped with rungs (Figure 7A; Video S1), allowing the precision of contralateral forepaw placements to be assessed, a motor task requiring motor cortex contributions in mice (Schiemann et al., 2015). Mice performed better on day 5 compared to day 1 (Figure 7B; $p < 0.05$, Friedman test). Interestingly, increasing $[K^+]_o$ in the motor cortex by changing the ACSF from 3.5 mM to 5 mM K^+, eliciting a ~0.7 mM increase in L2/3 $[K^+]_o$ (Figure S5), increased the percentage of correct paw placements (Figures 7C and 7D; $p < 0.05$, Wilcoxon signed-rank test) but did not change average running velocity (7.3 ± 0.6 cm/s and 5.8 ± 0.7 cm/s with 3.5 and 5 mM K^+, respectively, $p \geq 0.05$, Wilcoxon signed-rank test). In contrast, the percentage of correct paw placements did not differ between two consecutive sessions with application of 5 mM K^+ ACSF (Figures 7C and 7D; $p \geq 0.05$, Wilcoxon signed-rank test), and the motor performance enhancement with 5 mM K^+ could be recovered after reverting to 3.5 mM K^+ ACSF (Figure S6).

Output layers of the motor cortex project to midbrain, brain stem, and spinal cord motor circuits (Anderson et al., 2010; Drew and Marigold, 2015; Kiehn, 2016; Oswald et al., 2013).

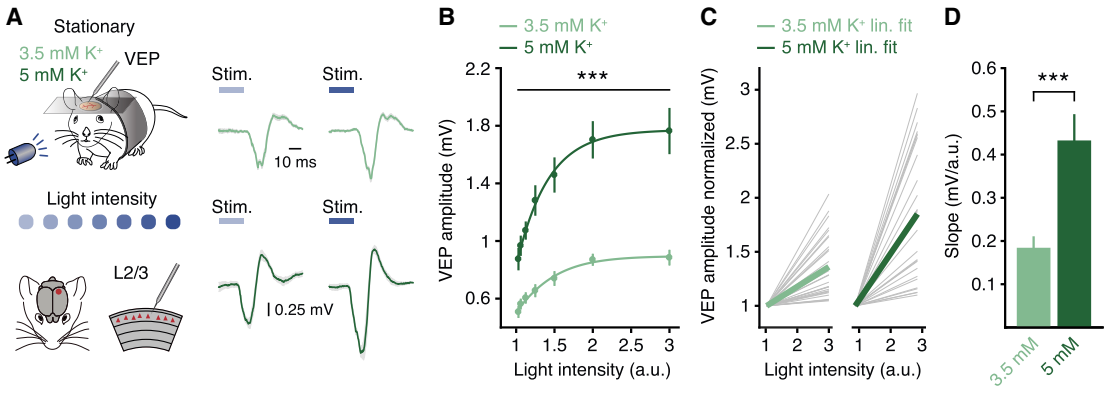

Figure 6. Increasing $[K^+]_o$ Recreates State-Dependent Gain Modulation in the Visual Cortex

(A) Left: VEPs were elicited in visual cortex L2/3 of awake stationary mice while visual cortex was covered with 3.5 mM or 5 mM K^+ ACSF. Right: example VEP traces with 3.5 mM (top) or 5 mM (bottom) K^+; blue bars denote visual stimulation; shading indicates SEM.

(B) VEP amplitude as a function of light intensity with 3.5 and 5 mM K^+. ***$p < 0.001$, n = 26 recordings, N = 5 mice, Wilcoxon signed-rank test; error bars are mean ± SEM and solid lines are sigmoid fit.

(C) Linear function fits to the normalized VEP amplitude as a function of light intensity for 3.5 mM and 5 mM K^+; individual fits are in gray and average is colored.

(D) Bar plot comparing slopes of linear function fits. ***$p < 0.001$, n = 26 recordings, N = 5 mice, Wilcoxon signed-rank test; error bars indicate SEM.

See also Figure S5.

Because increasing $[K^+]_o$ improved motor coordination, we proposed that neural activity in deep motor cortical layers might differ with varying $[K^+]_o$. To test this, we recorded single-unit activity (SUA) from motor cortex L5 (Figure S7), with 3.5 or 5 mM K^+ ACSF (Figure S5), while mice transitioned between being stationary and running on the runged treadmill (Figure 7E). Most units showed higher spike rates during running compared to stationary (Figure 7F). Increasing $[K^+]_o$ increased spike rates during running (Figures 7G–7I; $p < 0.001$, Wilcoxon rank-sum test), whereas spike rates did not significantly differ when mice were stationary (Figures 7G–7I; $p \geq 0.05$, Wilcoxon rank-sum test). Raising $[K^+]_o$ thus increased the ratio between running versus stationary spike rates (Figure 7J; $p < 0.01$, Wilcoxon rank-sum test), indicating motor cortical gain modulation. These results demonstrate that the level of $[K^+]_o$ has functional consequences on the spiking activity of motor cortex L5 neurons and skilled motor behavior.

DISCUSSION

Neural activity has long been known to be modulated by behavioral state, but the mechanism governing this effect is unclear. Across the cortex, $[K^+]_o$ exhibit stereotypic changes when mice transition between being stationary and locomotive, and manipulating $[K^+]_o$ affect sensory processing and motor outputs. Our analysis of cortical $[K^+]_o$ in behaving mice provide the first insight into understanding the role of $[K^+]_o$ for behavioral state-dependent neuronal function.

Role of $[K^+]_o$ in Cortical State-Dependent Neural Processing

During the transition from quiescence to active, the cortex shifts into a desynchronized state concurrently with a gain in responses to incoming visual inputs (Bennett et al., 2013; Dadarlat and Stryker, 2017; Neske and McCormick, 2018; Niell and Stryker, 2010; Polack et al., 2013). This mechanism likely evolved to support rapid and flexible adaptation to changes in the environment. A mechanism that globally affects cortical neural activity and amplifies sensory inputs is expected to be highly predictable and robust, since the awake brain constantly shifts back and forth between quiet and active states. *In vivo*, the V_m of neurons exhibits considerable variance. As a consequence, the relationship between V_m and spike rate in response to an input follows a power law (Anderson et al., 2000; Haider and McCormick, 2009; Miller and Troyer, 2002; Murphy and Miller, 2003). This means that tonic V_m depolarization can produce multiplicative gain modulation (Murphy and Miller, 2003). In fact, previous studies have shown that most cortical neurons depolarize by 2−4 mV when animals transition from being stationary to running (Bennett et al., 2013; McGinley et al., 2015; Polack et al., 2013; Reimer et al., 2014; Schiemann et al., 2015), and this depolarization is thought to drive gain modulation of visual responses during periods of arousal and alertness (Bennett et al., 2013; Polack et al., 2013) (Figure 5). Interestingly, the onset of this depolarization occurs 0.2−3 s before the onset of locomotion (Bennett et al., 2013; McGinley et al., 2015; Polack et al., 2013; Reimer et al., 2016; Schiemann et al., 2015; Schneider et al., 2014; Zhao et al., 2016). However, the mechanism driving this depolarization across the cortex is debated. Theoretical modeling has proposed that subtle changes in extracellular ion composition are sufficient for transitioning neurons into the active state (Rasmussen et al., 2017). Here, we report that, during behavioral state transitions, $[K^+]_o$ increases by 0.5−1 mM across the cortex (Figures 1, 2, 3, S1, and S2), capable of depolarizing cortical neurons by 4 mV in slices (Figure 4). The onset of this $[K^+]_o$ rise precedes the onset of running by ~1 s (Figures 1, 2, 3, S1, and S2). Artificially increasing local $[K^+]_o$ is sufficient to produce multiplicative gain modulation in the visual cortex in the absence of apparent behavioral state changes (Figure 6). Thus, when

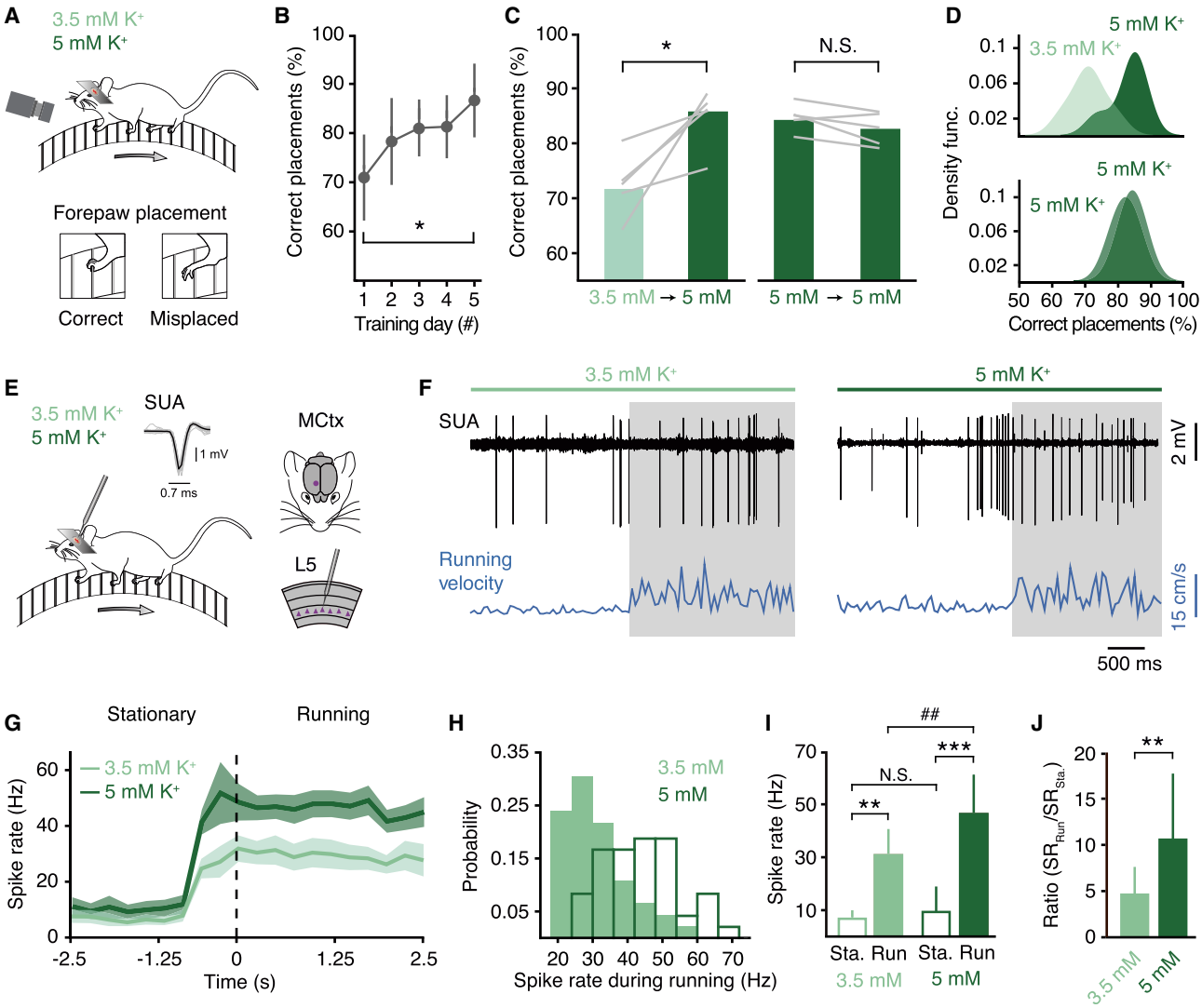

Figure 7. Raising Motor Cortex $[K^+]_o$ Improves Motor Performance and Amplifies L5 Spiking

(A) Mice transitioned between being stationary and running on a runged treadmill while video was acquired for scoring forepaw placements with 5 mM or 3.5 mM K^+ ACSF covering the motor cortex.

(B) Percentage of correct placements over training period. *$p < 0.05$, n = 5 mice, Friedman test; error bars are mean ± SEM.

(C) Percentage of correct placements with 3.5 and 5 mM K^+. *$p < 0.05$, N.S., not significant, $p \geq 0.05$, n = 5 mice, Wilcoxon signed-rank test; lines represent average shift for each mouse.

(D) Probability density functions of the percentage of correct placements using bootstrapping.

(E) SUA was recorded in motor cortex L5 while mice transitioned between being stationary and running; motor cortex was covered with 3.5 or 5 mM K^+ ACSF.

(F) Example traces of SUA and running activity with 3.5 or 5 mM K^+.

(G) Average spike rate aligned to running onset (n = 46 and 48 periods recorded from 17 and 18 units for 3.5 and 5 mM K^+, respectively, N = 5 mice); shading indicates SEM.

(H) Histogram depicting distribution of spike rates during running.

(I) Comparisons of spike rates during stationary and running periods. **$p < 0.01$, ***$p < 0.001$, n = 17 and 18 units for 3.5 and 5 mM K^+, respectively, N = 5 mice, Wilcoxon signed-rank test; N.S. $p \geq 0.05$, ##$p < 0.01$, n = 17 and 18 units for 3.5 and 5 mM K^+, respectively, N = 5 mice, Wilcoxon rank-sum test; error bars indicate SEM.

(J) Ratio of spike rates during running and stationary periods. **$p < 0.01$, n = 17 and 18 units for 3.5 and 5 mM K^+, respectively, N = 5 mice, Wilcoxon rank-sum test; error bars indicate SEM.

See also Figures S5–S7 and Video S1.

animals transition from quiet to active, a tonic increase in $[K^+]_o$ could be contributing to shifting the V_m of neurons by a few mV; this, in turn, at least in part, increases the gain of visually evoked responses, amplifying the response sensitivity to incoming streams of visual information when actively navigating in an often complex environment.

As in the visual cortex, we found that $[K^+]_o$ in the motor cortex increases consistently before and during locomotion (Figure 1), and raising $[K^+]_o$ increases the spiking of L5 neurons during movement execution while improving skilled motor performance (Figures 7 and S6). These findings are in consonance with previous work showing that L2/3 motor cortical neurons depolarize by 3–4 mV before and during the transition from stationary to running, and this depolarization is correlated with fine motor control (Schiemann et al., 2015). Interestingly, when $[K^+]_o$ in the motor cortex was increased, the ratio of spike rates during running versus being stationary was increased in L5 neurons (Figure 7), suggestive of $[K^+]_o$-mediated gain modulation. Supporting this notion, previous work found that a population of L5 neurons increases their gain during locomotion, and this gain increase was correlated with a tonic V_m depolarization (Schiemann et al., 2015). Thus, a cortex-wide increase in $[K^+]_o$ might act as a general mechanism by which cortical neurons can undergo gain modulation as a function of the ongoing behavioral state and contextual requirements.

Although the neural state change and $[K^+]_o$ increases are cortex-wide, not all neurons increase their sensory responsiveness during active behavior. In the barrel cortex, the sensory responses of L2/3 and L4 neurons to passively applied whisker stimulation are smaller during active compared to quiet states (Crochet and Petersen, 2006; Poulet and Crochet, 2019; Yamashita et al., 2013), and tone evoked responses in L2/3 excitatory neurons in auditory cortex are suppressed during locomotion (McGinley et al., 2015; Schneider et al., 2014; Zhou et al., 2014). To reconcile these findings with our present data, we propose a general mechanism where a cortex-wide increase in $[K^+]_o$ participates in shifting the V_m and amplifying the responsiveness of cortical neurons; this effect converges with neural circuit-specific mechanisms, such as the balance of excitatory and inhibitory synaptic barrages, short-term plasticity, neuromodulator signaling, and anatomical connectivity, ultimately scaling neural activity depending on the behavioral state and context.

Local Sources Contribute to State-Dependent Changes in Cortical $[K^+]_o$

Increases in $[K^+]_o$ may derive from barrages of neural activity (Brocard et al., 2013; Hounsgaard and Nicholson, 1983; Ransom et al., 2000; Shih et al., 2013) by means of K^+ efflux through voltage- and neurotransmitter-gated ion channels. Alternatively, $[K^+]_o$ may increase via a neural activity independent mechanism, controlled by neuromodulators (Ding et al., 2016). To dissect the mechanism orchestrating state-dependent $[K^+]_o$ changes, it is therefore important to probe the relationship between neural activity and $[K^+]_o$ in behaving mice. Here, we report that, in the presence of excitatory transmission antagonists, running-associated $[K^+]_o$ increases in L2/3 of the visual cortex is markedly diminished, but not abolished (Figure 3), suggesting that local neuronal activity notably contributes to state-dependent $[K^+]_o$ dynamics. This view is supported by *in vitro* experiments showing that NMDA receptor activation leads to $[K^+]_o$ efflux, which, in turn, causes synaptic facilitation via retrograde signaling (Shih et al., 2013). Furthermore, we found that MUA spiking and $[K^+]_o$ were well correlated, and $[K^+]_o$ was delayed by ~1.1 s relative to MUA spiking (Figure S4). This finding appears in congruence with our finding that state-dependent $[K^+]_o$ increases rose as a function of increasing baseline $[K^+]_o$ (Figure S2), suggesting that the overall excitability of the local neural network is an important determinant for the magnitude of $[K^+]_o$ increases during running. Interestingly, our findings appear to corroborate previous work showing that CNQX and AP5 application reduces, but does not prevent, the tonic depolarization of L2/3 neurons in the visual cortex when mice transition from being stationary to running: rather, a ~0.8 mV depolarization persists (Polack et al., 2013). This finding, together with the 0.4 mM running-associated increase in $[K^+]_o$ while neural activity was suppressed (Figure 3), seems to suggest that additional mechanisms are contributing to state-dependent $[K^+]_o$ changes. Although we cannot fully rule out that the remaining $[K^+]_o$ transient stems from incomplete blockage of AMPA and NMDA receptors, we consider this less likely since we used high concentrations of CNQX and AP5, identical to those previously employed *in vivo* (Mateo et al., 2011), and we allowed >30 min incubation before assessing the effect in L2/3 (Vinokurova et al., 2018), resulting in a more than 60% decrease in broadband LFP power (Figure S3). The remaining $[K^+]_o$ increase could instead originate from local spiking of axons projecting into superficial layers of V1, such as those from the lateral geniculate nucleus (Cruz-Martín et al., 2014; Roth et al., 2016; Sun et al., 2016). Alternatively, neuromodulators—in particular, norepinephrine and acetylcholine—have been implicated in mediating state-dependent cortical activity (Eggermann et al., 2014; Fu et al., 2014; Polack et al., 2013; Schiemann et al., 2015). Outside the CNS, norepinephrine and acetylcholine are well recognized for their role in regulating ion transport (Browning et al., 1977; Clausen and Flatman, 1977; Hildebrand and Brown, 1992; Hirota and McKay, 2006), and Ca^{2+} imaging from cholinergic or noradrenergic axons in the cortex during behavioral state transitions show a striking similarity to $[K^+]_o$ dynamics (Larsen et al., 2018; Reimer et al., 2016). Thus, one might speculate that another mechanism for increasing $[K^+]_o$ in the awake cortex is through concerted noradrenergic and cholinergic signaling, as was recently shown *in vitro* (Ding et al., 2016). Such a hypothesis has yet to be tested *in vivo*, but could be explored by local optogenetic activation of cholinergic or noradrenergic axons (Meir et al., 2018) while simultaneously measuring $[K^+]_o$ during local neural activity suppression.

Future Perspectives

Our $[K^+]_o$ recordings in behaving animals are the first to document state-dependent cortex-wide increases in $[K^+]_o$ when mice transition from quiet wakefulness to locomotion. Additional analysis indicated that the $[K^+]_o$ increases were potent for modulating both sensory gain and motor output and performance. In future studies, it will be of critical importance to investigate the contribution of $[K^+]_o$ in sensory processing in other cortical and extracortical areas than those studied here. Furthermore, it will be central to directly assess the causal role of $[K^+]_o$ in mediating brain state shifts and the role of $[K^+]_o$ in higher-order brain functions, such as attention and decision making. For this, the advent of new methodological tools allowing targeted and tempospatial precise manipulation of $[K^+]_o$ will be essential. Clearly,

our study is therefore only a first step toward a comprehensive description of $[K^+]_o$ during behavior.

STAR★METHODS

Detailed methods are provided in the online version of this paper and include the following:

- KEY RESOURCES TABLE
- LEAD CONTACT AND MATERIALS AVAILABILITY
- EXPERIMENTAL MODEL AND SUBJECT DETAILS
  - Animals
- METHOD DETAILS
  - Surgeries
  - Cylindrical treadmill setup
  - $[K^+]_o$ and LFP/MUA measurements
  - Manipulating $[K^+]_o$
  - Cortical slice preparation
  - Slice electrophysiology
  - Pharmacology
  - Visual stimulation and VEP recordings
  - Motor cortex SUA recordings
  - Motor coordination assessment
- QUANTIFICATION AND STATISTICAL ANALYSIS
  - Statistics
- DATA AND CODE AVAILABILITY

SUPPLEMENTAL INFORMATION

Supplemental Information can be found online at https://doi.org/10.1016/j.celrep.2019.06.082.

ACKNOWLEDGMENTS

We thank A.T. Nguyen for commenting on the manuscript, W. Song and N. Lou for technical assistance, A. Matsumoto for assistance with data analysis, and D. Xue for assistance with illustrations. This study was supported by the NIH/NINDS/NIA (AG048769, NS078394, and NS100366), the Lundbeck Foundation, the Novo Nordisk Foundation, and Dr. Miriam and Sheldon G. Adelson Medical Research Foundations.

AUTHOR CONTRIBUTIONS

R.R. and M.N. designed the experiments. R.R., E.N., N.C.P., A.G.D., and Q.W. conducted the experiments. R.R. and E.N. designed the analyses. R.R. performed the analyses. R.R. and M.N. wrote the paper with assistance from E.N.

DECLARATION OF INTERESTS

The authors declare no competing interests.

Received: March 13, 2019
Revised: June 1, 2019
Accepted: June 24, 2019
Published: July 30, 2019

REFERENCES

Anderson, J.S., Lampl, I., Gillespie, D.C., and Ferster, D. (2000). The contribution of noise to contrast invariance of orientation tuning in cat visual cortex. Science *290*, 1968–1972.

Anderson, C.T., Sheets, P.L., Kiritani, T., and Shepherd, G.M.G. (2010). Sublayer-specific microcircuits of corticospinal and corticostriatal neurons in motor cortex. Nat. Neurosci. *13*, 739–744.

Armstrong, D.M., and Drew, T. (1984). Discharges of pyramidal tract and other motor cortical neurones during locomotion in the cat. J. Physiol. *346*, 471–495.

Balestrino, M., Aitken, P.G., and Somjen, G.G. (1986). The effects of moderate changes of extracellular K+ and Ca2+ on synaptic and neural function in the CA1 region of the hippocampal slice. Brain Res. *377*, 229–239.

Bazhenov, M., Timofeev, I., Steriade, M., and Sejnowski, T.J. (2004). Potassium model for slow (2-3 Hz) in vivo neocortical paroxysmal oscillations. J. Neurophysiol. *92*, 1116–1132.

Bennett, C., Arroyo, S., and Hestrin, S. (2013). Subthreshold mechanisms underlying state-dependent modulation of visual responses. Neuron *80*, 350–357.

Brocard, F., Shevtsova, N.A., Bouhadfane, M., Tazerart, S., Heinemann, U., Rybak, I.A., and Vinay, L. (2013). Activity-dependent changes in extracellular Ca2+ and K+ reveal pacemakers in the spinal locomotor-related network. Neuron *77*, 1047–1054.

Browning, J.G., Hardcastle, J., Hardcastle, P.T., and Sanford, P.A. (1977). The role of acetylcholine in the regulation of ion transport by rat colon mucosa. J. Physiol. *272*, 737–754.

Castro-Alamancos, M.A. (2004). Absence of rapid sensory adaptation in neocortex during information processing states. Neuron *41*, 455–464.

Chance, F.S., Abbott, L.F., and Reyes, A.D. (2002). Gain modulation from background synaptic input. Neuron *35*, 773–782.

Cirelli, C. (2009). The genetic and molecular regulation of sleep: from fruit flies to humans. Nat. Rev. Neurosci. *10*, 549–560.

Cirelli, C., Bushey, D., Hill, S., Huber, R., Kreber, R., Ganetzky, B., and Tononi, G. (2005). Reduced sleep in Drosophila Shaker mutants. Nature *434*, 1087–1092.

Clausen, T., and Flatman, J.A. (1977). The effect of catecholamines on Na-K transport and membrane potential in rat soleus muscle. J. Physiol. *270*, 383–414.

Cotel, F., Exley, R., Cragg, S.J., and Perrier, J.-F. (2013). Serotonin spillover onto the axon initial segment of motoneurons induces central fatigue by inhibiting action potential initiation. Proc. Natl. Acad. Sci. USA *110*, 4774–4779.

Crochet, S., and Petersen, C.C.H. (2006). Correlating whisker behavior with membrane potential in barrel cortex of awake mice. Nat. Neurosci. *9*, 608–610.

Cruz-Martín, A., El-Danaf, R.N., Osakada, F., Sriram, B., Dhande, O.S., Nguyen, P.L., Callaway, E.M., Ghosh, A., and Huberman, A.D. (2014). A dedicated circuit links direction-selective retinal ganglion cells to the primary visual cortex. Nature *507*, 358–361.

Dadarlat, M.C., and Stryker, M.P. (2017). Locomotion Enhances Neural Encoding of Visual Stimuli in Mouse V1. J. Neurosci. *37*, 3764–3775.

Ding, F., O'Donnell, J., Xu, Q., Kang, N., Goldman, N., and Nedergaard, M. (2016). Changes in the composition of brain interstitial ions control the sleep-wake cycle. Science *352*, 550–555.

Dombeck, D.A., Graziano, M.S., and Tank, D.W. (2009). Functional clustering of neurons in motor cortex determined by cellular resolution imaging in awake behaving mice. J. Neurosci. *29*, 13751–13760.

Drew, T., and Marigold, D.S. (2015). Taking the next step: cortical contributions to the control of locomotion. Curr. Opin. Neurobiol. *33*, 25–33.

Drew, T., Prentice, S., and Schepens, B. (2004). Cortical and brainstem control of locomotion. Prog. Brain Res. *143*, 251–261.

Eggermann, E., Kremer, Y., Crochet, S., and Petersen, C.C.H. (2014). Cholinergic signals in mouse barrel cortex during active whisker sensing. Cell Rep. *9*, 1654–1660.

Fröhlich, F., Bazhenov, M., Iragui-Madoz, V., and Sejnowski, T.J. (2008). Potassium dynamics in the epileptic cortex: new insights on an old topic. Neuroscientist *14*, 422–433.

Fu, Y., Tucciarone, J.M.M., Espinosa, J.S.S., Sheng, N., Darcy, D.P.P., Nicoll, R.A.A., Huang, Z.J.J., and Stryker, M.P.P. (2014). A cortical circuit for gain control by behavioral state. Cell *156*, 1139–1152.

Haider, B., and McCormick, D.A. (2009). Rapid neocortical dynamics: cellular and network mechanisms. Neuron *62*, 171–189.

Harris, K.D., and Thiele, A. (2011). Cortical state and attention. Nat. Rev. Neurosci. *12*, 509–523.

Hildebrand, K.R., and Brown, D.R. (1992). Norepinephrine and alpha-2 adrenoceptors modulate active ion transport in porcine small intestine. J. Pharmacol. Exp. Ther. *263*, 510–519.

Hirota, C.L., and McKay, D.M. (2006). Cholinergic regulation of epithelial ion transport in the mammalian intestine. Br. J. Pharmacol. *149*, 463–479.

Hounsgaard, J., and Nicholson, C. (1983). Potassium accumulation around individual purkinje cells in cerebellar slices from the guinea-pig. J. Physiol. *340*, 359–388.

Kiehn, O. (2016). Decoding the organization of spinal circuits that control locomotion. Nat. Rev. Neurosci. *17*, 224–238.

Krishnan, G.P., González, O.C., and Bazhenov, M. (2018). Origin of slow spontaneous resting-state neuronal fluctuations in brain networks. Proc. Natl. Acad. Sci. USA *115*, 6858–6863.

Larsen, R.S., Turschak, E., Daigle, T., Zeng, H., Zhuang, J., and Waters, J. (2018). Activation of neuromodulatory axon projections in primary visual cortex during periods of locomotion and pupil dilation. bioRxiv. https://doi.org/10.1101/502013.

Lee, S.-H.H., and Dan, Y. (2012). Neuromodulation of brain states. Neuron *76*, 209–222.

Lemke, S.M., Ramanathan, D.S., Guo, L., Won, S.J., and Ganguly, K. (2019). Emergent modular neural control drives coordinated motor actions. Nat. Neurosci. *22*, 1122–1131.

Mateo, C., Avermann, M., Gentet, L.J., Zhang, F., Deisseroth, K., and Petersen, C.C.H. (2011). In vivo optogenetic stimulation of neocortical excitatory neurons drives brain-state-dependent inhibition. Curr. Biol. *21*, 1593–1602.

McGinley, M.J., David, S.V., and McCormick, D.A. (2015). Cortical Membrane Potential Signature of Optimal States for Sensory Signal Detection. Neuron *87*, 179–192.

Meir, I., Katz, Y., and Lampl, I. (2018). Membrane Potential Correlates of Network Decorrelation and Improved SNR by Cholinergic Activation in the Somatosensory Cortex. J. Neurosci. *38*, 10692–10708.

Miller, K.D., and Troyer, T.W. (2002). Neural noise can explain expansive, power-law nonlinearities in neural response functions. J. Neurophysiol. *87*, 653–659.

Miri, A., Warriner, C.L., Seely, J.S., Elsayed, G.F., Cunningham, J.P., Churchland, M.M., and Jessell, T.M. (2017). Behaviorally Selective Engagement of Short-Latency Effector Pathways by Motor Cortex. Neuron *95*, 683–696.e11.

Murphy, B.K., and Miller, K.D. (2003). Multiplicative gain changes are induced by excitation or inhibition alone. J. Neurosci. *23*, 10040–10051.

Neske, G.T., and McCormick, D.A. (2018). Distinct waking states for strong evoked responses in primary visual cortex and optimal visual detection performance. bioRxiv. https://doi.org/10.1101/437681.

Niell, C.M., and Stryker, M.P. (2010). Modulation of visual responses by behavioral state in mouse visual cortex. Neuron *65*, 472–479.

Octeau, J.C., Gangwani, M.R., Allam, S.L., Tran, D., Huang, S., Hoang-Trong, T.M., Golshani, P., Rumbell, T.H., Kozloski, J.R., and Khakh, B.S. (2019). Transient, Consequential Increases in Extracellular Potassium Ions Accompany Channelrhodopsin2 Excitation. Cell Rep. *27*, 2249–2261.e7.

Orlovsky, G.N., Deliagina, T.G., and Grillner, S. (1999). Neuronal Control of Locomotion: From Mollusc to Man (Oxford Scholarship Online).

Oswald, M.J., Tantirigama, M.L.S., Sonntag, I., Hughes, S.M., and Empson, R.M. (2013). Diversity of layer 5 projection neurons in the mouse motor cortex. Front. Cell. Neurosci. *7*, 174.

Otazu, G.H., Tai, L.-H., Yang, Y., and Zador, A.M. (2009). Engaging in an auditory task suppresses responses in auditory cortex. Nat. Neurosci. *12*, 646–654.

Polack, P.O., Friedman, J., and Golshani, P. (2013). Cellular mechanisms of brain state-dependent gain modulation in visual cortex. Nat. Neurosci. *16*, 1331–1339.

Poolos, N.P., Mauk, M.D., and Kocsis, J.D. (1987). Activity-evoked increases in extracellular potassium modulate presynaptic excitability in the CA1 region of the hippocampus. J. Neurophysiol. *58*, 404–416.

Poulet, J.F.A., and Crochet, S. (2019). The Cortical States of Wakefulness. Front. Syst. Neurosci. *12*, 64.

Poulet, J.F.A., and Petersen, C.C.H. (2008). Internal brain state regulates membrane potential synchrony in barrel cortex of behaving mice. Nature *454*, 881–885.

Poulet, J.F.A., Fernandez, L.M.J., Crochet, S., and Petersen, C.C.H. (2012). Thalamic control of cortical states. Nat. Neurosci. *15*, 370–372.

Ransom, C.B., Ransom, B.R., and Sontheimer, H. (2000). Activity-dependent extracellular K+ accumulation in rat optic nerve: the role of glial and axonal Na+ pumps. J. Physiol. *522*, 427–442.

Rasmussen, R., Jensen, M.H., and Heltberg, M.L. (2017). Chaotic Dynamics Mediate Brain State Transitions, Driven by Changes in Extracellular Ion Concentrations. Cell Syst. *5*, 591–603.e4.

Reimer, J., Froudarakis, E., Cadwell, C.R., Yatsenko, D., Denfield, G.H., and Tolias, A.S. (2014). Pupil fluctuations track fast switching of cortical states during quiet wakefulness. Neuron *84*, 355–362.

Reimer, J., McGinley, M.J., Liu, Y., Rodenkirch, C., Wang, Q., McCormick, D.A., and Tolias, A.S. (2016). Pupil fluctuations track rapid changes in adrenergic and cholinergic activity in cortex. Nat. Commun. *7*, 13289.

Roth, M.M., Dahmen, J.C., Muir, D.R., Imhof, F., Martini, F.J., and Hofer, S.B. (2016). Thalamic nuclei convey diverse contextual information to layer 1 of visual cortex. Nat. Neurosci. *19*, 299–307.

Schiemann, J., Puggioni, P., Dacre, J., Pelko, M., Domanski, A., van Rossum, M.C.W., and Duguid, I. (2015). Cellular mechanisms underlying behavioral state-dependent bidirectional modulation of motor cortex output. Cell Rep. *11*, 1319–1330.

Schneider, D.M., Nelson, A., and Mooney, R. (2014). A synaptic and circuit basis for corollary discharge in the auditory cortex. Nature *513*, 189–194.

Shih, P.Y., Savtchenko, L.P., Kamasawa, N., Dembitskaya, Y., McHugh, T.J., Rusakov, D.A., Shigemoto, R., and Semyanov, A. (2013). Retrograde synaptic signaling mediated by K+ efflux through postsynaptic NMDA receptors. Cell Rep. *5*, 941–951.

Somjen, G.G. (2004). Ions in the Brain: Normal Function, Seizures, and Stroke (Oxford University Press).

Sun, W., Tan, Z., Mensh, B.D., and Ji, N. (2016). Thalamus provides layer 4 of primary visual cortex with orientation- and direction-tuned inputs. Nat. Neurosci. *19*, 308–315.

Tatsuki, F., Sunagawa, G.A., Shi, S., Susaki, E.A., Yukinaga, H., Perrin, D., Sumiyama, K., Ukai-Tadenuma, M., Fujishima, H., Ohno, R., et al. (2016). Involvement of Ca(2+)-Dependent Hyperpolarization in Sleep Duration in Mammals. Neuron *90*, 70–85.

Tong, X., Ao, Y., Faas, G.C., Nwaobi, S.E., Xu, J., Haustein, M.D., Anderson, M.A., Mody, I., Olsen, M.L., Sofroniew, M.V., and Khakh, B.S. (2014). Astrocyte Kir4.1 ion channel deficits contribute to neuronal dysfunction in Huntington's disease model mice. Nat. Neurosci. *17*, 694–703.

Vinokurova, D., Zakharov, A.V., Lebedeva, J., Burkhanova, G.F., Chernova, K.A., Lotfullina, N., Khazipov, R., and Valeeva, G. (2018). Pharmacodynamics of the Glutamate Receptor Antagonists in the Rat Barrel Cortex. Front. Pharmacol. *9*, 698.

Wang, F., Xu, Q., Wang, W., Takano, T., and Nedergaard, M. (2012). Bergmann glia modulate cerebellar Purkinje cell bistability via Ca2+-dependent K+ uptake. Proc. Natl. Acad. Sci. USA *109*, 7911–7916.

Wilson, D.E., Whitney, D.E., Scholl, B., and Fitzpatrick, D. (2016). Orientation selectivity and the functional clustering of synaptic inputs in primary visual cortex. Nat. Neurosci. *19*, 1003–1009.

Yamashita, T., Pala, A., Pedrido, L., Kremer, Y., Welker, E., and Petersen, C.C.H. (2013). Membrane potential dynamics of neocortical projection neurons driving target-specific signals. Neuron *80*, 1477–1490.

Yoshida, K., Shi, S., Ukai-Tadenuma, M., Fujishima, H., Ohno, R.-I., and Ueda, H.R. (2018). Leak potassium channels regulate sleep duration. Proc. Natl. Acad. Sci. USA *115*, E9459–E9468.

Zagha, E., Ge, X., and McCormick, D.A. (2015). Competing Neural Ensembles in Motor Cortex Gate Goal-Directed Motor Output. Neuron *88*, 565–577.

Zhao, W.J., Kremkow, J., and Poulet, J.F.A. (2016). Translaminar Cortical Membrane Potential Synchrony in Behaving Mice. Cell Rep. *15*, 2387–2399.

Zhou, M., Liang, F., Xiong, X.R., Li, L., Li, H., Xiao, Z., Tao, H.W., and Zhang, L.I. (2014). Scaling down of balanced excitation and inhibition by active behavioral states in auditory cortex. Nat. Neurosci. *17*, 841–850.

STAR★METHODS

KEY RESOURCES TABLE

REAGENT or RESOURCE	SOURCE	IDENTIFIER
Chemicals, Peptides, and Recombinant Proteins		
Dimethylsilane	Sigma	Cat# 144207
Potassium Ionophore 1-Cocktail B	Sigma	Cat# 99373
CNQX	Tocris Bioscience	Cat# 0190
AP5	Tocris Bioscience	Cat# 0106
Gabazine	Tocris Bioscience	Cat# 1262
Experimental Models: Organisms/Strains		
C57BL/6J mouse line	Charles River	Strain code: 027
Software and Algorithms		
MATLAB (versions used: 2015b and 2016a)	MathWorks	https://se.mathworks.com/
Clampfit	Molecular Devices	https://www.moleculardevices.com/
Spike2	CED	http://ced.co.uk/products/spkovin
Other		
KWIK-CAST	WPI	Item#: KWIK-CAST
Single-barreled glass microelectrodes	Sutter	B150-117-10
Vertical microelectrode puller	Narishige	PC-100 Puller
Head stages	Molecular Devices	CV-7B
Amplifier	Molecular Devices	MultiClamp 700B
Digitizer	Molecular Devices	Digidata 1440A
Magnetic encoder	US Digital	MAE3
Vibratome	Leica	VT1000S
Upright microscope	Olympus	BX51WI
Tungsten bipolar electrode	WPI	Cat #TST33C05KT
Pulse generator	A.M.P.I	Master-8
Amplifier	Warner Instruments	DP-311
Digitizer	Cambridge Electronic Design	Power1401
CMOS high-speed camera	Thorlabs	DCC3240N

LEAD CONTACT AND MATERIALS AVAILABILITY

This study did not generate new unique reagents. Further information and requests for resources and reagents should be directed to and will be fulfilled by the Lead Contact, Maiken Nedergaard (maiken_nedergaard@urmc.rochester.edu).

EXPERIMENTAL MODEL AND SUBJECT DETAILS

Animals

All experiments carried out at University of Rochester Medical Center complied with the NIH Guide for the Care and Use of Laboratory Animals and in accordance with guidelines approved by the institute ethics committee for the care and use of animals. All experiments performed at the University of Copenhagen were approved by the Danish National Animal Experiment Committee and were in accordance with European Union Regulations. Animals were wild-type C57BL/6J mice aged 8–12 weeks of either sex (Charles River), maintained on a 12-hour light/dark cycle. Mice were kept in individually ventilated cages with bedding and nesting material. Health monitoring was according to FELASA Guideline 2014.

METHOD DETAILS

Surgeries

A lightweight metal plate was affixed to the skull using a combination of cyanoacrylate and dental cement under isoflurane (1.5%) anesthesia. Mice were allowed to recover for 2–3 days following surgery and were then accustomed to head fixation in the experimental setup on the treadmill. Mice received no reward during or after training sessions; they were neither food- nor water-deprived before placed on the treadmill. After 3–5 days of habituation, circular craniotomies with the dura left intact were performed above motor, visual or sensory cortex (2–3 mm in diameter) under isoflurane anesthesia using stereotactic coordinates (motor cortex: 0.13–1 mm anterior, 1.5–2 mm lateral; visual cortex: 3–4 mm posterior, 2.5–3 mm lateral; and sensory cortex: 1–1.5 mm posterior, 3–3.5 mm lateral, all relative to bregma), and the cortical surface was thereafter kept moist with standard ACSF containing (mM): 125, NaCl 3.5 KCl, 1 $CaCl_2$, 0.8 $MgCl_2$, 10 HEPES. Animals were allowed to recover for 60 min prior to recordings, time during which the craniotomy was covered with a silicon elastomer (KWIK-CAST, WPI) to protect the cortical tissue.

Cylindrical treadmill setup

To record locomotor activity we custom-built a cylindrical treadmill equipped with a magnetic rotary encoder (MAE3 Absolute Magnetic Kit Encoder, US DIGITAL) mounted on the treadmill axis to record angular position at a sampling rate of 10 kHz (synchronized to $[K^+]_o$ and LFP signals). The encoder generated an output of 0–5 V, corresponding to 0° to 360°. Afterward, we transformed the 0–5 V signal into linear velocity (cm/s) and this measure was used for all further analyses. The percentage of time mice spent walking/running (velocity > 1 cm/s) varied from mouse to mouse, but was approximately 35–45% overall. To determine the onset of running, the treadmill velocity trace was first filtered with a moving median filter (window size: 30 data points). Next, the filtered trace was binarized using a threshold definition of 1 cm/s (Niell and Stryker, 2010) and all running onset time points determined. To prevent running bouts where $[K^+]_o$ had not fully returned back to baseline being analyzed, we only used running onsets > 30 s after the end of the preceding running period: this value was based on the empirical observation that $[K^+]_o$ returned fully to baseline within ~8–10 s of the mouse stopping running.

$[K^+]_o$ and LFP/MUA measurements

To detect changes in K^+ in the extracellular environment we made K^+-sensitive microelectrodes as previously described (Ding et al., 2016; Wang et al., 2012). In brief, single-barreled glass microelectrodes (1.17/1.5 inner/outer diameter, Sutter Instruments) were pulled to a tip size of < 2–3 μm using a vertical puller (PC-100, Narishige Japan). Microelectrodes were silanized with dimethylsilane (Fluka, Sigma) and loaded with an ~300 μm column of valinomycin-based K^+ ion-exchange resin at the tip (potassium ionophore I - cocktail B, Fluka, Sigma), and backfilled with 150 mM KCl. The reference microelectrode, used for measuring the LFP and MUA, was filled with standard ACSF. The two microelectrodes were connected to head stages (CV-7B, Axon Instruments) of a MultiClamp 700B amplifier (Axon Instruments) and the signals digitized with an Axon Digidata 1440A digitizer (Axon Instruments). The microelectrodes were calibrated in 2.5, 3.5 and 4.5 mM K^+ ACSF before and after all experiments, and typical voltage responses were 5–6 mV per 1 mM change in K^+ concentration. The microelectrodes were positioned 150–300 μm (L2/3) or 500–1000 μm (L5) below the pial surface and with ~50 μm between the tips of the microelectrodes. Both $[K^+]_o$ and LFP/MUA signals were acquired at 10 kHz using Clampex 10.2 software (Axon Instruments). To convert the acquired voltage signal into $[K^+]_o$ (mM), custom-made MATLAB procedures employing a modified Nikolsky equation (Ding et al., 2016; Wang et al., 2012) were used:

$$[K^+]_o = 150 \times 10^{\wedge}((E_{subtraced}\text{-}E_o)/m) \quad (1)$$

Where $[K^+]_o$ is the extracellular K^+ concentration (mM); 150 is the concentration of KCl (mM) backfilled into the microelectrode; $E_{subtracted}$ is the voltage signal from the K^+ electrode subtracted the voltage signal from the reference electrode (mV); E_0 is the electrode offset (mV); and *m* is the slope of the regression line constructed from the standard solutions (2.5, 3.5, and 4.5 mM K^+ ACSF). In brief, first the reference signal was subtracted from the K^+-sensitive signal to cancel out any DC shifts, yielding $E_{subtracted}$. Next, the offset (E_0) and slope (*m*) of the linear regression line were determined from the standard curve measurements, and the full $E_{subtracted}$ signal converted into mM using Equation 1. Afterward the $[K^+]_o$ signal was down-sampled to 200 Hz. The raw, broadband LFP signal was obtained by band-pass filtering the signal from the reference electrode between 0.1–100 Hz using a 5th order Butterworth filter and afterward down-sampled to 200 Hz. For sample 1–4 Hz LFP traces, the raw broadband LFP was further band-pass filtered using a Butterworth filter. To determine LFP power content, we used the *bandpower* function and afterward converted the signal into dB using the *pow2 db* function in MATLAB. MUA was determined by band-pass filtering the signal from the reference electrode between 300–3000 Hz using a 5th order Butterworth filter (Zagha et al., 2015). MUA spikes were afterward determined as threshold crossings well isolated from the background noise (> 2 × amplitude), and spike rates were obtaining by summing spikes in 10 ms time bins.

Manipulating $[K^+]_o$

This method was adapted from a previous publication that tested the causal implications of extracellular ion changes on neural activity (Ding et al., 2016). To reproduce the precise running-associated shift in $[K^+]_o$, we conducted exploratory experiments to determine the shift in $[K^+]_o$, resulting from changing the K^+ content of ACSF topically applied over the cortex. Based on this result,

we designed two ACSF solutions: one mimicking $[K^+]_o$ measured in stationary mice and the other increasing $[K^+]_o$ by 0.5–0.8 mM (mean: 0.73 mM) as observed during running. "Stationary ACSF" contained (in mM): 125 NaCl, 3.5 KCl, 1 $CaCl_2$, 0.8 $MgCl_2$, 10 HEPES; "Running ACSF" contained (in mM): 123.5 NaCl, 5 KCl, 1 $CaCl_2$, 0.8 $MgCl_2$, 10 HEPES. The effect of these two solutions on $[K^+]_o$ in L2/3 and L5 was validated using K^+-sensitive microelectrodes (Figure S5). Additionally, in a subset of experiments, we measured $[K^+]_o$ dynamics during behavioral state changes with 0 mM K^+ ACSF covering the cortex (Figure S2). For this we used ACSF containing (in mM): 128.5 NaCl, 0 KCl, 1 $CaCl_2$, 0.8 $MgCl_2$, 10 HEPES. The same approach was used to design the two ACSF solutions for slice experiments. We conducted exploratory experiments to determine the shift in $[K^+]_o$ 50–100 μm below the slice surface resulting from altering the K^+ concentration in the ACSF superfusing the slice. One solution mimicked the $[K^+]_o$ measured when mice were stationary and one increased $[K^+]_o$ by 0.5–0.8 mM, as measured during running. "Stationary slice ACSF" contained (in mM): 126 NaCl, 3.5 KCl, 2 $CaCl_2$, 2 $MgCl_2$, 26 $NaHCO_3$, 1.25 NaH_2PO_4, and 10 glucose; "Running slice ACSF" contained (in mM): 125 NaCl, 4.5 KCl, 2 $CaCl_2$, 2 $MgCl_2$, 26 $NaHCO_3$, 1.25 NaH_2PO_4, and 10 glucose. The effect of these two solutions on $[K^+]_o$ in cortical slices was validated using K^+-sensitive microelectrodes (Figure S5).

Cortical slice preparation

All slices used for $[K^+]_o$ measurements and whole-cell patch-clamp recordings were prepared as described previously (Ding et al., 2016; Wang et al., 2012). In brief, mice were anesthetized using 3.5% isoflurane in a closed chamber, decapitated, and whole brains rapidly extracted and immersed in ice-cold cutting solution containing the following (mM): 230 sucrose, 2.5 KCl, 0.5 $CaCl_2$, 10 $MgCl_2$, 26 $NaHCO_3$, 1.25 NaH_2PO_4, and 10 glucose. Coronal cortical slices containing sensory or motor areas (300 μm thick) were prepared using a vibratome (Leica VT1000S). Slices were then transferred to beakers containing oxygenated standard slice ACSF containing (mM): 126 NaCl, 2.5 KCl, 2 $CaCl_2$, 2 $MgCl_2$, 26 $NaHCO_3$, 1.25 NaH_2PO_4, and 10 glucose. Slices were here incubated for 1-5 h at room temperature before being used for recordings. For measuring $[K^+]_o$ in cortical slices, the same overall procedure as used *in vivo* was employed, with microelectrodes positioned 50–100 μm below the surface of the slice and the tips < 10 μm apart.

Slice electrophysiology

Whole-cell patch clamp experiments in slices were performed as previously described (Wang et al., 2012). All recordings from cortical L2/3 pyramidal neurons were obtained at a depth of 50–100 μm below the surface of the slice. Membrane potentials (V_m) were recorded under the current-clamp configuration with a MultiClamp 700B amplifier (Axon Instruments), low-pass filtered at 8 kHz, and digitized at 20 kHz with an Axon Digidata 1440A digitizer (Axon Instruments). No bias currents were injected ($I = 0$) unless indicated. Patch microelectrodes typically had a resistance of 6–8 MΩ when filled with internal solution containing (mM): 140 K-gluconate, 5 Na-phosphocreatine, 2 $MgCl_2$, 10 HEPES, 4 Mg-ATP, and 0.3 Na-GTP, pH adjusted to 7.3 using KOH. Cells were visualized with differential interference contrast optics on an upright microscope (BX51WI, Olympus). Distance to spike threshold was determined as the voltage difference between the resting V_m and the spike threshold, located as the kink in the spike waveform (Wilson et al., 2016). To determine input resistance we applied repeated +10 mV voltage steps (500 ms duration, 1 s between steps) in the voltage-clamp configuration, i.e., stepping the V_m from −80 mV to −70 mV, and then offline measured the amplitude of the responding change in current. From Ohm's law we then calculated the input resistance in both 3.5 and 4.5 mM K^+ ACSF. To measure excitability we performed five consecutive depolarization current in the current-clamp configuration of 140 pA (pulse duration 300 ms). The holding potential was initially set at −80 mV when the slice was superfused with 3.5 mM K^+ ACSF. Data analysis was performed offline in MATLAB using standard custom-made procedures.

Pharmacology

For *in vivo* experiments employing excitatory glutamatergic antagonists, these were purchased from Tocris (CNQX 0190, AP5 0106) and dissolved in standard 3.5 mM K^+ ACSF on the day of experiment from concentrated aliquots to final concentrations of 0.8 mM and 1.6 mM for CNQX and AP5, respectively (Mateo et al., 2011). CNQX/AP5 was topically applied with 30 min incubation before evaluating the effect (Vinokurova et al., 2018). For cortical slice experiments, glutamatergic antagonists were dissolved in standard ACSF on the day of experiment from concentrated aliquots, to final concentrations of 20 μM and 50 μM for CNQX and AP5, respectively (Cotel et al., 2013). To block fast inhibitory GABAergic synaptic transmission in slice experiments, Gabazine was purchased from Tocris (SR 95531 hydrobromide) and dissolved in standard ACSF on the day of the experiment from concentrated aliquots to a final concentration of 10 μM (Cotel et al., 2013).

Visual stimulation and VEP recordings

For visual stimulation experiments, we stimulated the contralateral eye of awake mice with a 20 ms whole-field light flash from a 430 nm LED (Prizmatix) placed at a consistent height and distance from the eye. The visual-evoked potential (VEP) triggered was recorded using an ACSF-filled glass microelectrode and sampled at 20 kHz. Averages of responses to visual stimulation were calculated from 6-8 trials of stimulation at each light intensity level, with an interstimulus interval of 30 s. In experiments manipulating $[K^+]_o$ we randomly applied ACSF containing either 3.5 or 5 mM K^+ to the craniotomy, and afterward switched to ACSF with the other K^+ concentration. To categorize visual stimulation trials into "stationary" and "running" in the awake, spontaneously running mice, we used the running activity as a discriminator. In brief, recordings were acquired in event-triggered sweep-mode, with each sweep having a length of 30 s, with 15 s of data recorded before the light stimulation. To designate a sweep as "running," the treadmill velocity at

the time of the visual stimulation onset had to exceed 1 cm/s; otherwise the sweep was categorized as ''stationary.'' To assess VEP gain, we measured the amplitude of the early, short-latency negative voltage deflection of the VEP. To probe multiplicative-like gain modulation we used the slope of linear functions fitted to each input-output curve (i.e., light intensity versus voltage amplitude), and compared slopes across experimental groups. Additive gain was expected to change the absolute VEP amplitudes, without affecting the input-output curve slopes, whereas multiplicative-like gain was expected to change both the absolute VEP amplitudes as well as the slope of input-output curves.

Motor cortex SUA recordings

SUA spiking measurements were obtained with ACSF-filled glass microelectrodes (resistance 6-8 MΩ) connected to a DP-311 differential amplifier (Warner Instruments) and sampled at 20 kHz using a power1401 digitizer (Cambridge Electronic Design) and Spike2 software (CED, UK) through a small (~1 mm) craniotomy prepared above motor cortex (with the dura carefully removed). SUA recordings were targeted to L5 at depths ranging from 500−1000 μm below the cortical surface and obtained by slowly advancing the microelectrode while monitoring the voltage signal. The SUA signal was band-pass filtered between 300 and 3000 Hz. Afterward, analyses were conducted in MATLAB; spikes were determined as threshold crossings well isolated from the background noise (> 2 × amplitude) (Zagha et al., 2015); and finally aligned to onset of running on the runged treadmill (see details in section below). Mean spike rate curves were obtained by summing spikes in 200 ms bins and averaging across running periods. Resting spike rate was determined as the average spike rate 2.5−2 s before running onset, and running spike rate as the average spike rate 0−0.5 s after running onset.

Motor coordination assessment

To assess motor coordination, mice were head-restrained and accustomed over 5−6 days to walk/run on a cylindrical treadmill equipped with rungs similarly to previously reported (Schiemann et al., 2015) (Video S1). Contralateral forepaw placements were recorded at 100 frames per second using a high sensitivity CMOS camera (Model: DCC324N, Thorlabs), and were post hoc scored independently and classified as either precise or misplaced (Schiemann et al., 2015). On the day of the experiment, a 3 mm craniotomy was prepared above motor cortex and mice placed on the runged treadmill. After 60 min of recovery (KWIK-CAST protecting the cortical tissue during this period), video sequences were captured while the craniotomy was bathed in ACSF containing either 5 or 3.5 mM K^+ (30 min incubation). We randomly first applied ACSF containing 3.5 or 5 mM K^+ to the craniotomy, and afterward switched to the other concentration. For the control group experiments, instead of changing the ACSF from one concentration to the other, we re-applied ACSF containing the same K^+ concentration, keeping the total time on the treadmill the same between experimental groups. To depict the variance of the underlying forepaw placement accuracy, 10000 bootstrap samples (randomly sampled with replacement) from each population were taken, and bootstrap samples plotted as the probability density estimate using the *ksdensity* function in MATLAB.

QUANTIFICATION AND STATISTICAL ANALYSIS

Statistics

All group comparisons were performed using two-sided non-parametric Wilcoxon signed-rank or Wilcoxon rank-sum tests. The non-parametric Kruskal-Wallis test with a Dunn's multiple comparisons post hoc test was used to compare multiple groups. To test the null-hypothesis that the population median value is 0 we used the one-sample signed-rank test. To test for normally distributed data, we used the one-sample Kolmogorov-Smirnov test. To test if two distributions differed we used the two-sample Kolmogorov-Smirnov test. Correlation coefficients were computed using Pearson's correlation test. Data plotted in figures are shown as mean ± SEM unless otherwise stated. We used no statistical methods to plan sample sizes, but used sample sizes similar to those frequently used in the field. Statistical significance was considered with p values < 0.05, with asterisks marking: *p < 0.05, **p < 0.01, and ***p < 0.001.

DATA AND CODE AVAILABILITY

The published article includes all datasets generated or analyzed during this study. All code used for analysis are available upon request.